

Galaxy-galaxy lensing: dissipationless simulations versus the halo model

Rachel Mandelbaum^{1*}, Argyro Tasitsiomi², Uroš Seljak^{1,3}, Andrey V. Kravtsov^{2,4}, Risa H. Wechsler^{2,5}

¹*Department of Physics, Princeton University, Princeton, NJ 08544, USA*

²*Department of Astronomy & Astrophysics, Kavli Institute for Cosmological Physics, The University of Chicago, Chicago, IL 60637, USA*

³*International Centre for Theoretical Physics, Strada Costiera 11, 34014 Trieste, Italy*

⁴*Enrico Fermi Institute, The University of Chicago*

⁵*Hubble Fellow, Enrico Fermi Fellow*

1 December 2021

ABSTRACT

Galaxy-galaxy lensing is a powerful probe of the relation between galaxies and dark matter halos, but its theoretical interpretation requires a careful modeling of various contributions, such as the contribution from central and satellite galaxies. For this purpose, a phenomenological approach based on the halo model has been developed, allowing for fast exploration of the parameter space of models. In this paper, we investigate the ability of the halo model to extract information from the g-g weak lensing signal by comparing it to high-resolution dissipationless simulations that resolve subhalos. We find that the halo model reliably determines parameters such as the host halo mass of central galaxies, the fraction of galaxies that are satellites, and their radial distribution inside larger halos. If there is a significant scatter present in the central galaxy host halo mass distribution, then the mean and median mass of that distribution can differ significantly from one another, and the halo model mass determination lies between the two. This result suggests that when analyzing the data, galaxy subsamples with a narrow central galaxy halo mass distribution, such as those based on stellar mass, should be chosen for a simpler interpretation of the results.

Key words: galaxies: halos – methods: analytical

1 INTRODUCTION

Understanding the connection between the spatial distribution of galaxies and dark matter (DM) is one of the most important problems in modern cosmology. From the perspective of fundamental physics, this connection needs to be understood if we wish to use galaxy clustering to determine dark matter correlations, a potentially powerful discriminator between cosmological models. This connection can also be a powerful test of the tenets of the standard cosmological paradigm, such as the collisionless nature of cold dark matter. From the astrophysics perspective, this connection is an essential ingredient in the physics of galaxy formation. Current models based on pure N-body simulations, semi-analytic models or hydrodynamic simulations can accommodate many observational aspects of this connection, but several ingredients of these models remain uncertain and need to be inserted ad-hoc, so it is not clear how much of the success is a result of the allowed freedom within these models.

It is important to look for new ways to test this connection, to confirm and improve the existing models of structure formation, and to distinguish astrophysical effects from cosmological ones.

One of the probes of the galaxy-DM connection that recently became available is weak lensing around galaxies, or galaxy-galaxy (hereinafter g-g) lensing (Tyson et al. 1984; Brainerd et al. 1996; Hudson et al. 1998; Fischer, et al. 2000; Smith et al. 2001; McKay, et al. 2001; Hoekstra et al. 2003; Sheldon et al. 2004; Hoekstra et al. 2004; Seljak et al. 2005). Gravitational lensing induces tangential shear distortions of background galaxies around foreground galaxies, allowing direct measurement of the galaxy-dark matter correlation function around galaxies. The individual distortions are small (of order 0.1%), but by averaging over all foreground galaxies within a given subsample, we obtain high signal to noise in the shear as a function of angular separation from the galaxy. If we know the galaxy redshifts, the shear signal can be related to the projected mass density as a function of proper distance from the galaxy. This allows

* Electronic address: rmandelb@princeton.edu

us to determine statistically the dark matter distribution around any given galaxy sample.

In recent years, the progress on the observational side of g-g lensing has been remarkable. In the latest Sloan Digital Sky Survey (SDSS) analyses (Sheldon et al. 2004; Seljak et al. 2005), 20-30 sigma detections of the signal as a function of physical separation have been obtained. Similarly high S/N detections have also been observed as a function of angular separation with other surveys (Hoekstra et al. 2004). This increased statistical power has been accompanied by a more careful investigation of systematic errors, such as calibration biases and intrinsic correlations, which for the SDSS are currently around 10% and therefore already dominate the error budget (Hirata et al. 2004). As the quality and quantity of the data and its analysis improves, the reliability of theoretical interpretation must be improved as well. The goal of the present paper is to compare the various theoretical analyses among themselves, and to discuss how they should be applied to the data.

Theoretical analysis of g-g lensing falls into two categories. The first approach is a direct comparison of simulations to the data (Guzik & Seljak 2001; Yang et al. 2003; Weinberg et al. 2004; Tasitsiomi et al. 2004). This approach is direct, but rather expensive, since the process of galaxy formation is not understood sufficiently well to result in unique predictions for a given cosmological model, nor is the cosmological model itself determined yet. Moreover, current simulations still suffer from a limited dynamical range, in the sense that they require a high mass and force resolution to resolve individual galaxies and their associated dark matter halos, while at the same time they must also have sufficiently large volume to simulate a representative region of the universe. Several simulations of varying box size are needed to cover the whole observational range in luminosity and scale. As a result, many different simulations would be needed to explore the whole range of parameter space; at present, only a handful of simulations have been used for this application.

The second approach is to use the halo model (for a review, see Cooray & Sheth 2002) to describe the connection between galaxies and dark matter (Guzik & Seljak 2002, hereinafter GS02). This approach is more phenomenological, and for a given galaxy class leads to determination of quantities such as the virial mass distribution and the fraction of these galaxies that are satellites, which are useful quantities for constraining the galaxy formation models and cosmological models. While the information extracted from the data using the halo model may be all that is needed to quantify the galaxy-dark matter connection, halo models are reliable only to the extent that they are able to reproduce the simulations, so they must be tested and calibrated on the simulations before applications to the real data are reliable.

In this paper, we attempt to understand how well the phenomenological halo model developed in Seljak (2000) and studied in GS02 can reproduce the simulations. We are interested in its ability to reproduce the g-g lensing signal, which in turn can be used to determine the halo mass probability distribution, the radial profile of satellite galaxies inside larger halos, and other quantities of interest.

2 SIMULATIONS

We use simulations described in Tasitsiomi et al. (2004), where the reader can find further details. We assume the concordance flat Λ CDM model: $\Omega_m = 1 - \Omega_\Lambda = 0.3$, $h = 0.7$, where Ω_m and Ω_Λ are the present-day matter and vacuum densities, and h is the dimensionless Hubble constant defined as $H_0 \equiv 100h \text{ km s}^{-1} \text{ Mpc}^{-1}$. The power spectrum normalization is $\sigma_8 = 0.9$. The model is consistent with recent observational constraints (e.g., Spergel et al. 2003; Tegmark, et al. 2004). The effects of the power spectrum normalization, box size and cosmic variance were studied in Tasitsiomi et al. (2004) using a range of simulation box sizes. Given current constraints, it is impossible to achieve the desired level of precision across the entire range of luminosities probed by the observations. Small box sizes can achieve sufficient mass resolution to resolve very small halos, but the sampling variance due to large scale fluctuations is large, which results in large errors on predictions at scales above a few hundred kpc. To reduce sampling errors, we will choose the largest box available from the simulations in Tasitsiomi et al. (2004), a $120 h^{-1} \text{ Mpc}$ box with 512^3 particles. The particle mass of this simulation is $m_p = 1.07 \times 10^9 h^{-1} M_\odot$, so only halos with virial mass above a few times $10^{11} h^{-1} M_\odot$ are resolved. For this reason, we will restrict the analysis to galaxies brighter than $M_r = -19$.

The simulations were run using the Adaptive Refinement Tree N -body code (ART; Kravtsov et al. 1997; Kravtsov & Klypin 1999). The ART code reaches high force resolution by refining all high-density regions with an automated refinement algorithm. The criterion for refinement is the mass of particles per cell. The initial grid is 1024^3 and the refinement criterion is level- and time-dependent. At the early stages of evolution ($a < 0.65$) the thresholds are set to 2, 3, and 4 particle masses for the zeroth, first, and second and higher levels, respectively. At low redshifts, $a > 0.65$, the thresholds for these refinement levels are set to 6, 5, and 5 particle masses. The lower thresholds at high redshifts are set to ensure that collapse of small-mass halos is followed with higher resolution. The maximum achieved level of refinement is $L_{\max} = 8$. As a function of redshift the maximum level of refinement is equal to $L_{\max} = 6$ for $5 < z < 7$, $L_{\max} = 7$ for $1 < z < 5$, $L_{\max} \geq 8$ for $z < 1$. The peak formal resolution is $h_{\text{peak}} \leq 1.8 h^{-1} \text{ kpc}$ (physical).

A variant of the Bound Density Maxima halo finding algorithm (Klypin et al. 1999) is used to identify halos and the subhalos within them. The details of the algorithm and parameters used in the halo finder can be found in Kravtsov et al. (2004). The main steps of the algorithm are the identification of local density peaks (potential halo centers) and analysis of the density distribution and velocities of the surrounding particles to test whether a given peak corresponds to a gravitationally bound clump. More specifically, density, circular velocity, and velocity dispersion profiles are constructed around each potential halo center. The unbound particles are then removed iteratively using the procedure outlined in Klypin et al. (1999). The final profiles are constructed using only bound particles. We use these profiles to calculate properties of halos, such as the circular velocity profile $V_{\text{circ}}(r) = \sqrt{GM(< r)/r}$, and compute the maximum circular velocity V_{\max} .

In this study, we distinguish between *host halos* with

centers that do not lie within any larger virialized system, and *subhalos* (or *satellites*) located within the virial radii of larger systems. We associate the former with central galaxies and the latter with non-central galaxies or satellites. To classify the halos, we calculate the formal boundary of each object as the radius corresponding to an enclosed overdensity of 180 with respect to the mean density of the universe. Note that we do not consider the center of a host halo to be a subhalo. Thus, host halos may or may not contain any subhalos with circular velocity above the threshold of a given sample. The host centers, however, are included in clustering statistics because we assume that each host harbors a *central galaxy* at its center. Therefore, the total sample of galactic halos contains central and satellite galaxies. The former have the positions and maximum circular velocities of their host halos, while the latter have the positions and maximum circular velocities of subhalos. In a cluster, for example, the brightest central galaxy that typically resides near the center would be associated with the cluster host halo in our terminology. All other galaxies within the virial radius of the cluster would be considered “satellites” associated with subhalos.

Our galaxy sample is created by assigning realistic SDSS luminosities and colors to dark matter halos. To construct mock galaxy catalogs for comparison with observations, one must define selection criteria for particular halo properties to mimic the selection function of the observational sample as closely as possible. Halo mass is often used to define halo catalogs; e.g., a catalog can be constructed by selecting all halos in a given mass range. However, the mass and radius are poorly defined for the satellite halos due to tidal stripping, which alters a halo’s mass and physical extent (see Klypin et al. 1999). Therefore, we use the maximum circular velocity, V_{\max} , as a proxy for the halo mass. For isolated halos, V_{\max} and the halo’s virial mass are directly related. For subhalos, V_{\max} will experience secular decrease but at a relatively slow rate (Kravtsov et al. 2004).

To mimic the observational selection function, r -band luminosities are assigned to the halos as follows. We match the cumulative velocity function $n(> V_{\max})$ of the halos to the SDSS observed r -band cumulative luminosity function (Blanton, et al. 2003). Note that $n(> V_{\max})$ includes both isolated host halos and subhalos. We use the r -band data since that band was used for SDSS spectra selection, has a more reliable luminosity function measurement observationally, and is the focus of most SDSS analyses. We first obtain the average $V_{\max} - M_r$ relation by matching $n(> V_{\max})$ to $n(< M_r)$. This was the same method used to assign luminosities to subhalos in Kravtsov et al. (2004), in which galaxy clustering properties were reproduced remarkably well. The mean redshift of the lens galaxies is 0.1, so we use halo catalogs at this redshift.

One may also introduce scatter in the relation between V_{\max} and M_r , which here we have chosen as a Gaussian in M_r at fixed V_{\max} , as described in detail in Tasitsiomi et al. (2004). The amplitude and dependence of the scatter on galaxy luminosity or halo mass are very uncertain, so here we will simply explore this example to investigate its consequences. The value of scatter is meant to be realistic for the current data, which are a mixture of early and late type galaxies and for which intrinsic reddening corrections have not been applied. The Gaussian scatter is introduced

in a fashion that keeps the luminosity function constant, which results in somewhat lower scatter for higher luminosity galaxies and vice versa. Below we present extensive comparisons of the halo model and the actual simulation results with and without scatter.

3 OVERVIEW OF THE HALO MODEL

3.1 Dark matter halos

In current cosmological models, structure grows hierarchically from small, initially Gaussian fluctuations. Once the fluctuations go nonlinear, they collapse into virialized halos. The spatial density of halos as a function of their mass M is specified by the halo mass function dn/dM , which in general is a function of redshift z . It can be written as

$$\frac{dn}{dM} dM = \frac{\bar{\rho}}{M} f(\nu) d\nu, \quad (1)$$

where $\bar{\rho}$ is the mean matter density of the universe. We introduced the function $f(\nu)$, which can be expressed in units in which it has a theoretically universal form independent of the power spectrum or redshift if written as a function of peak height

$$\nu = \left[\frac{\delta_c}{\sigma(M)} \right]^2. \quad (2)$$

Here $\delta_c = 1.686$ is the linear overdensity at which a spherical perturbation collapses at redshift z , and $\sigma(M)$ is the rms fluctuation in spheres that contain on average mass M at an initial time, extrapolated using linear theory to z .

The first analytic model for the mass function was proposed by Press & Schechter (1974). While it correctly predicts the abundance of massive halos, it overpredicts the abundance of halos around and below the nonlinear mass scale $M_{\text{nl}}(z)$ (defined below). An improved version has been proposed by Sheth & Tormen (1999),

$$\nu f(\nu) = A(1 + \nu'^{-p})\nu'^{1/2}e^{-\nu'^{1/2}}, \quad (3)$$

where $\nu' = a\nu$, with $a = 0.707$ and $p = 0.3$ as the best fit values (the Press & Schechter (1974) mass function corresponds to $a = 1$, $p = 0$). Further modifications to this expression have been suggested in Yahagi et al. (2004), but the effects are very small and we will ignore them here. The constant A is determined by mass conservation, requiring that the integral over the mass function times the mass gives the mean density or, equivalently, $\int f(\nu)d\nu = 1$. It has been shown that the form in equation 3 can be derived analytically within the framework of the ellipsoidal collapse model (Sheth et al. 2001). For a given peak height, we can also compute the bias

$$b(\nu) = 1 + \frac{\nu' - 1}{\delta_c} + \frac{2p}{\delta_c(1 + \nu'^p)}, \quad (4)$$

where for the purpose of computing the bias we use $a = 0.73$ and $p = 0.15$ rather than the values from the mass function, in order to best match the results from Seljak & Warren (2004). As shown in Fig. 2 of Warren, et al. (2005), the original Sheth & Tormen (1999) mass function and this modified one give nearly identical results in the most relevant range of halo masses, $10^{11}\text{--}10^{14} h^{-1} M_{\odot}$. In support of this assertion, we note that when we compare the predicted halo model

lensing signal computed with the two mass functions, the difference is less than 1 per cent.

The halo mass is defined in terms of the linking length parameter of the friends-of-friends (FoF) algorithm, which is 0.2 for the simulations used in Sheth & Tormen (1999). This definition roughly corresponds to spherical overdensity halos of 180 times the background density (Jenkins et al. 2001; White 2001). For the range of masses of interest here and their corresponding halo concentrations, it is about 30–35% larger than the mass defined as the mass within the radius where the density is 200 times the critical density. Since we use $\Omega_m = 0.3$ when computing the virial masses, they are defined as the mass within the radius in which the mean density is 54 times the critical density. We will also define the concentration parameter relative to this radius.

3.2 Halo-galaxy connection and galaxy-galaxy lensing

In the current paradigm of structure formation, all galaxies form inside dark matter halos. While this is generally accepted, we also know that the relation between the two is not one-to-one, and galaxies of the same luminosity can be found in halos of different masses. For example, a typical galaxy like the Milky Way may be found at the center of a low mass halo with a typical size 200 kpc, it may be part of a small group with typical size 500 kpc or it may be a satellite in a cluster with a typical size of 1-2 Mpc. We wish therefore to determine the probability ΔP for a galaxy in this sample to be in a halo of mass $M \pm \Delta M/2$. To describe this probability, we will use the conditional halo mass probability distribution $dP/dM \equiv p(M; L)$ (GS02). With g-g lensing, one can in principle determine the full halo mass function, since small halos contribute only at small scales, while large halos such as clusters also generate signal at larger scales. The fact that g-g lensing measures the signal over a wide range of scales facilitates the determination of the full halo mass function for a given subsample. In practice, given the measurement errors, a model must be adopted to extract this information from the data.

Galaxy-galaxy lensing measures the tangential shear distortions in the shapes of background galaxies induced by the mass distribution around foreground galaxies. Because the shear distortions γ_t are very small, in our case 10^{-3} , while the typical galaxy shape noise is 0.3, we must average over many foreground-background pairs to extract the signal. The result is a measurement of the shear-galaxy cross-correlation as a function of relative foreground-background separation on the sky. We will assume that the redshift of the foreground galaxy is known, so one can express the relative separation in terms of transverse comoving scale R . If, in addition, the redshift distribution of the background galaxies, or their actual redshifts, are known, then one can relate the shear distortion γ_t to $\Delta\Sigma(R) = \bar{\Sigma}(< R) - \Sigma(R)$, where $\Sigma(R)$ is the surface mass density at the transverse separation R and $\bar{\Sigma}(< R)$ its mean within R , via

$$\gamma_t = \frac{\Delta\Sigma(R)}{\Sigma_{\text{crit}}}. \quad (5)$$

Here

$$\Sigma_{\text{crit}} = \frac{c^2}{4\pi G} \frac{r_s}{(1+z_L)r_L r_{LS}}, \quad (6)$$

where r_L and r_s are the comoving distances to the lens and source, respectively, r_{LS} is the comoving distance between the two and z_L is the redshift of the lens. If only the probability distribution for source redshifts is known, then this expression needs to be integrated over. In principle, the relation between comoving distance and measured redshift depends on cosmology, but since we are dealing with low redshift objects, varying cosmology within the allowed range makes little difference. We will assume a cosmology with $\Omega_m = 0.3$ and $\Omega_\Lambda = 0.7$, and we work in comoving coordinates throughout the paper.

We will first overview the halo model formalism of GS02, beginning the discussion with a simplified description. Let us assume that a given halo of mass M produces an average lensing profile $\Delta\Sigma(R, M)$. This can be obtained via line of sight integration over the dark matter profile, which in this paper is modeled as a NFW profile (Navarro et al. 1996)

$$\rho(r) = \frac{\rho_s}{(r/r_s)(1+r/r_s)^2}. \quad (7)$$

This model assumes that the profile shape is universal in units of the scale radius r_s , while its characteristic density ρ_s or concentration $c_{\text{dm}} = r_v/r_s$ may depend on the halo mass, which here will be modeled as (Bullock et al. 2001; Eke et al. 2001)

$$c_{\text{dm}} = 10 \left(\frac{M}{M_{\text{nl}}(z)} \right)^{-0.13}. \quad (8)$$

$M_{\text{nl}}(z)$, which depends on the cosmology, is defined such that the rms linear density fluctuation, extrapolated to redshift z , within a sphere containing mass M_{nl} is equal to δ_c . Since most of the signal is at $R > 50 - 100 h^{-1}$ kpc, baryonic effects can be neglected (see, e.g., Gnedin et al. 2004), dark matter profiles are well determined from simulations, and concentration or the choice of the halo profile does not play a major role. The average g-g lensing signal for a galaxy with luminosity L is

$$\langle \Delta\Sigma \rangle(R; L) = \int p(M; L) \Delta\Sigma(R, M) dM. \quad (9)$$

Because of noise in the g-g lensing signal, we cannot invert the relation to obtain the conditional mass probability distribution with arbitrary precision, but instead assume some functional form for it and fit for its parameters.

Our simplified description so far ignores the fact that there are two distinct galaxy types that need to be modeled separately. The first type are the galaxies that formed at the centers of dark matter halos, such as the so-called field galaxies or cD galaxies in the cluster centers. The second type are the non-central galaxies, or satellites. We know that a galaxy of a given luminosity can be of either type, so following GS02, we split $p(M; L)$ into two parts, p^C and p^{NC} , representing respectively central and non-central galaxies, with the fraction of non-central galaxies in each luminosity bin L_i given by a free parameter α_i :

$$p(M; L_i) = (1 - \alpha_i) p^C(M; L_i) + \alpha_i p^{NC}(M; L_i). \quad (10)$$

α_i is, by definition, the satellite fraction determined for the given lens sample as a whole.

For the central galaxy population we assume that the relation between the halo mass and galaxy luminosity is

tight and we model this component with a delta-function,

$$p^C(M; L_i) dM = \delta^D(M - M_{0,i}) dM, \quad (11)$$

where $M_{0,i}$ is the typical halo mass of the i th luminosity bin. In reality, this component should have some width both because of intrinsic scatter in the $M - L$ relation, scatter due to inclination and dust, and because we work with luminosity bins of finite width. Explicit tests have shown that the results are only weakly affected even if the scatter is a factor of 2-3 in mass (GS02). If the scatter is larger, then the effects can be larger; we will use simulations to investigate this effect.

The non-central galaxies are different in that they have presumably formed in smaller halos which then merged into larger ones. It is thus reasonable to assume that their luminosity is not related to the final (host) halo mass. Instead we assume a relation between the number of these non-central galaxies and the halo mass: the larger the halo, the more satellites of a given luminosity one expects to find in it. We assume this relation is a power law, $\langle N \rangle(M; L) \propto M^\epsilon$, above some minimal halo mass M_{\min} , which should be larger than the halo mass of the central galaxy component above, since we are assuming that there is already another galaxy at the halo center. Below this cutoff, the number of galaxies quickly goes to zero. These assumptions imply

$$p^{NC}(M; L_i) dM \propto F(M) M^{\epsilon_i} \frac{dn}{dM} dM. \quad (12)$$

GS02 used $F(M) = \Theta^H(M - M_{\min,i})$ where $M_{\min,i} = 3M_{0,i}$; here, we will use a slightly more realistic functional form that is smoother than the step function and matches the simulations better. This is described in more detail in the next section. We have verified that the two expressions do not yield significantly different results. Semi-analytic models of galaxy formation (Kauffmann et al. 1999, GS02), subhalos in N-body simulations (Kravtsov et al. 2004), and direct observational measurements (Lin et al. 2004; Zehavi, et al. 2004) agree with this model, and predict that for most galaxies, $\epsilon \sim 1$ and $\alpha \sim 0.2$. In fact, when attempting to fit for both ϵ and α , we find that these two parameters are almost completely degenerate. We therefore assume fixed $\epsilon = 1$, and do not fit for it throughout this study.

For the non-central component, the weak lensing profile $\Delta\Sigma(R, M)$ is a convolution of the halo profile with the radial distribution of the galaxies. Since we are explicitly excluding the central galaxies, the non-central galaxy component of the g-g lensing signal does not peak at the center. Instead, for a given halo mass, it is small at small radii, peaks at a fraction of the virial radius, and drops off at large radii.

We assume that the radial distribution of galaxies is proportional to the dark matter profile, $c_g = a c_{dm}$. Observationally, there is not much evidence for any departures from $a = 1$, but the constraints are weak and only exist for clusters (Carlberg et al. 1997). As a result, a could differ significantly from unity, as discussed in more detail in Nagai & Kravtsov (2005). We will show that g-g lensing may be a useful way to measure it observationally for groups as well.

On scales below $2h^{-1}\text{Mpc}$, the one-halo or Poisson term dominates the g-g lensing signal. As shown in GS02, the lensing signal from neighboring halos (called the “halo-halo” or hh term) can be neglected for $R < 2h^{-1}\text{Mpc}$, while on very

large scales this term dominates and follows linear theory. For the sake of consistency between results on large and small scales, we have included it here. Since the NFW profile is not abruptly truncated at the virial radius in simulations, we have investigated the dependence of the results on the maximum radius to which the halo profile is integrated in, e.g., equation 14. We define this radius in units of the virial radius, so $x_1 = 1$ means that no mass beyond the virial radius is taken into account. (This is only true for the non-central term; when computing the Poisson term due to the central halo, the profile is not truncated at $x_1 r_{vir}$ when projecting to get $\Sigma(R)$ from $\rho(r)$.) Since we do not assume that the halo mass function accounts for all the mass in the universe, there is no concern of double-counting mass when using $x_1 > 1$. The halo-halo correlations also depend on the large scale bias, which for a given halo mass distribution is given by equation 4. Unfortunately, the small box size of the simulations implies that the sampling variance is important on large scales, so the errors on large scales may be underestimated. They are also highly correlated, and our fits do not take the correlation into account. Nonetheless, we perform fits out to $13 h^{-1}\text{Mpc}$, keeping in mind that the errorbars are actually larger due to the correlations, and that the bias is somewhat degenerate with the choice of x_1 . Based on our investigations, we see no reason to include mass beyond the virial radius, and so use $x_1 = 1$ throughout this work, but larger simulations will be necessary to investigate the behavior on large scales in more depth.

In addition to correlations of satellite galaxies with the host halo dark matter, there are correlations between a satellite galaxy and dark matter particles of its own (sub)halo. Thus, the remaining uncertainty in modeling satellites is how much of the dark matter around satellite galaxies remains attached to them. Analyses of cosmological simulations show that the typical fraction of mass bound to subhalos is $\approx 0.1 - 0.2$, roughly independent of the host halo mass but strongly dependent on the distance from the host center (e.g., Ghigna et al. 1998; Gao et al. 2004; Weller et al. 2004). Since the fraction of subhalos, α , is typically low ($\alpha \sim 0.2$), the correction due to the subhalo bound mass is small. The fraction of dark matter remaining is likely to depend on the details of satellite history, such as the point of closest approach to the halo center, where the tidal stripping is strongest. It is also likely to be somewhat correlated with the instantaneous position of the satellite, but this correlation is not perfect, given the highly elliptical orbits of satellites observed in simulations (Ghigna et al. 2000). Determining this position in all but the most massive clusters (where the center is often traced by either X-ray emission or a cD galaxy) is difficult. For this reason, we will work with an average quantity rather than some function of radial distance from the halo center. We assume the dark matter was tidally stripped in the outer parts of the halo, but remains unmodified in the inner parts of the satellite halo. Effectively this means that each non-central galaxy also has a central contribution, which we model in the same way as for the central galaxies (i.e., as a halo with mass $M_{0,i}$ before stripping) out to a fraction of virial radius, but totally stripped beyond that, yielding g-g lensing signal $\Delta\Sigma \propto R^{-2}$. Based on fits (figure 6) we will choose the truncation radius at $0.4r_{vir}$, which is equivalent to having 50% of the mass stripped, consistent with the average mass loss for subhalos.

los observed in cosmological simulations (Gao et al. 2004; Nagai & Kravtsov 2005). We note, however, that given existing measurement errors, the g-g lensing signal is only weakly sensitive to the exact value. Note that this truncation is responsible for the kink in the stripped satellite profile in the noncentral signal in figure 1; a more realistic approach might involve smoothing out this feature.

3.3 Signal computation

Using all of the above ingredients, we compute the predicted signal $\Delta\Sigma(R, M)$ for a given cosmological model and central halo mass M_0 , central galaxy bias $b(M_0)$, and c_g . Here we briefly describe the signal computation for the various contributions. Note that when we compute signal in comoving coordinates, the characteristic redshift z_0 is only used when computing the growth factor $b(z_0)$ for use in normalizing the linear power spectrum, and when determining $M_{\text{nl}}(z)$.

First, there is the 1-halo (Poisson) term for the central galaxies, $\Delta\Sigma_0^P$. This term can simply be computed by finding $\Sigma(R)$ and then $\Delta\Sigma(R)$ for a NFW profile given M_0 and c_{dm} which is determined from equation 8. When combining the signal from central and satellite galaxies, this term is multiplied by $1 - \alpha$. There is also a similar term for the satellites, $\Delta\Sigma_{\text{sat}}^P$, which assumes a stripped density profile. This term is the same as that for the central galaxies out to $0.4r_{\text{vir}}$ (our chosen truncation radius), then is proportional to R^{-2} beyond that scale. When combining signal for central and satellite galaxies, this term is multiplied by α .

For the remaining terms in the signal, $\Delta\Sigma$ was computed by finding the galaxy-dark matter cross power spectrum (this approach is described in Seljak (2000)). The power spectrum can then be Fourier transformed to obtain the galaxy-dark matter cross-correlation function $\xi_{g, \text{dm}}$, which yields $\Sigma(R)$ via an integration over the comoving separation

$$\Sigma(R) = \bar{\rho} \int \xi_{g, \text{dm}}[(R^2 + \chi^2)^{1/2}] d\chi \quad (13)$$

(where we have dropped an unobservable constant term) and $\Delta\Sigma(R)$ after another integration. The power spectrum can be related to the Fourier transform of the halo profile via $y(k, M)$, where

$$y(k, M) = \frac{\tilde{\rho}(k, M)}{M} = \frac{1}{M} \int_0^{x_1 r_{\text{vir}}} 4\pi r^2 dr \rho(r, M) \frac{\sin(kr)}{kr} \quad (14)$$

We can define y_g , the Fourier transform of the radial profile of galaxies using a NFW profile with concentration c_g , and y_{dm} , the Fourier transform of the halo dark matter profile with concentration c_{dm} .

This procedure was used to get the noncentral Poisson term $\Delta\Sigma_{\text{nc}}^P$, which is obtained from

$$P_{\text{nc}}^P(k) = \frac{1}{(2\pi)^3 \bar{n}} \int f(\nu) d\nu \langle N(M) \rangle y_{\text{dm}}(k, M) y_g(k, M) \quad (15)$$

and describes the correlations between satellite galaxies and their host halo dark matter. Because this is a noncentral term, it must be multiplied by α when computing its contribution to $\Delta\Sigma$.

This procedure was also used to compute the central and noncentral halo-halo terms, $\Delta\Sigma_{\text{cent}}^{hh}$ and $\Delta\Sigma_{\text{nc}}^{hh}$, which

dominate on large scales. The power spectrum for the central halo-halo term (describing correlations between the central galaxy of one host halo and the dark matter of another host halo), is

$$P_{\text{cent}}^{hh}(k) = b(M_0) P_{\text{lin}}(k) \int f(\nu) d\nu b(\nu) y_{\text{dm}}(k, M) \quad (16)$$

where the integration over ν includes all values. Note that dark matter must on average not be biased, and therefore the last term for a general $b(\nu)$ must reduce to 1 on large scales where $y_k = 1$. For the bias expression used in this paper, equation 4, the average bias is 1.06 rather than 1, but in order to reproduce the relation $P_{\text{cent}}^{hh}(k) = b(M_0) P_{\text{lin}}(k)$ on large scales, we have artificially normalized the integral to 1 on large scales. This central halo-halo power spectrum must be multiplied by $(1 - \alpha)$ when combining the signal for a mixture of central and noncentral galaxies.

For the remaining noncentral halo-halo term, we have

$$P_{\text{nc}}^{hh}(k) = P_{\text{lin}}(k) \int f(\nu) d\nu b(\nu) y_{\text{dm}}(k, M) \times \frac{\bar{\rho}}{\bar{n}} \int f(\nu) d\nu b(\nu) \frac{\langle N(M) \rangle}{M} y_g(k, M), \quad (17)$$

where the first integral, as above, must be 1 on large scales, and the second term can be normalized via

$$\frac{\bar{n}}{\bar{\rho}} = \int f(\nu) d\nu \frac{\langle N(M) \rangle}{M}$$

and (once normalized) equals the average bias $\langle b \rangle$ for satellite galaxies of this mass. Consequently, $P_{\text{nc}}^{hh}(k)$ reduces to $\langle b \rangle P_{\text{lin}}(k)$ on large scales, and must be multiplied by α when combining signal for central and satellite galaxies. When the central and noncentral signal are combined, we then have on large scales an effective bias $b_{\text{eff}} = (1 - \alpha)b(M_0) + \alpha\langle b \rangle$.

To illustrate the effects of the various contributions to the signal discussed in this section, figure 1 shows the predicted central (top), noncentral (middle) and total (bottom) signal for $\Omega_m = 0.3$, $\sigma_8 = 0.9$, $b(M_0) = 0.8$, and $M_0 = 5 \times 10^{12} h^{-1} M_{\odot}$. The central signal is the sum of two contributions:

$$\Delta\Sigma_{\text{cent}} = \Delta\Sigma_{\text{cent}}^P + \Delta\Sigma_{\text{cent}}^{hh} \quad (18)$$

and the satellite signal is the sum of three contributions:

$$\Delta\Sigma_{\text{sat}} = \Delta\Sigma_{\text{sat}}^P + \Delta\Sigma_{\text{nc}}^P + \Delta\Sigma_{\text{nc}}^{hh}. \quad (19)$$

For the combined signal we used satellite fraction $\alpha = 0.2$.

4 HALO MODEL VERSUS SIMULATIONS

As described in the introduction, the main motivation for the comparison between the halo model and simulations is that the halo model makes several approximations, so it must be verified and calibrated on realistic simulations. We may, of course, find that the simulations reproduce the data perfectly, in which case one could argue that the halo model itself is unnecessary. However, there may be different cosmological models or different treatments of how to populate halos and subhalos with galaxies that all agree equally well with the data. Rather than identify them with many expensive numerical simulations, one can use the halo model to do the same.

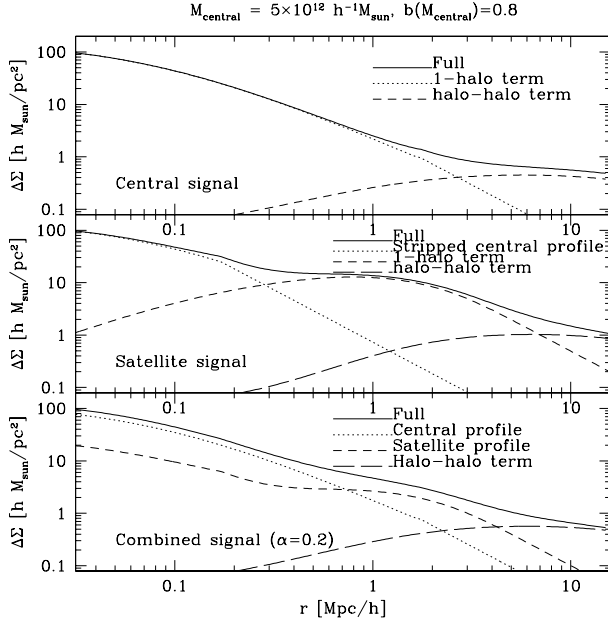


Figure 1. Halo model predictions for $\Delta\Sigma(r)$ for a central halo mass of $M_0 = 5 \times 10^{12} h^{-1} M_\odot$. The top panel shows the central signal with the 1-halo and halo-halo terms shown separately, assuming $b(M_0) = 0.8$. The middle panel shows the noncentral signal, with the stripped satellite central profile, the 1-halo non-central term, and the halo-halo noncentral term shown separately. The bottom panel shows the combined signal, with satellite fraction $\alpha = 0.2$.

As discussed in §2, the simulations used here cannot reliably resolve low mass halos, so we restrict our analysis to 3 luminosity bins, each 1 magnitude wide in r -band, L3 $[-19, -20]$, L4 $[-20, -21]$ and L5 $[-21, -22]$, using the notation from Seljak et al. (2005). We do not use the brightest bin (L6 $[-22, -23]$), since most of these galaxies reside in clusters, and our simulation box is too small to properly sample these.

To test how well g-g lensing analysis can extract various halo model parameters, we take the full g-g lensing signal from simulations and fit for 4 parameters: M_0 , $b(M_0)$, satellite fraction α , and radial distribution of satellites c_g . When performing the fits to the central galaxy signal alone, we also explored the sensitivity to the dark matter halo concentration parameter c_{dm} . We assign errors to the radial points using the actual errors that we find in SDSS analysis (Seljak et al. 2005). As the survey continues to take data, the error amplitude will decrease, but the relative errors will remain the same, so one can simply rescale the errors by the appropriate amount. Note, however, that a deeper survey, such as RCS (Hoekstra et al. 2004), can provide better information on g-g lensing at small radii, which would be particularly useful for determination of the halo concentration parameter c_{dm} .

Figure 2 shows the lensing signal $\Delta\Sigma(R)$ as a function of transverse separation R from the simulations, together with the halo model signal that fits the simulations best. We show the results separately for all luminosity bins with and without scatter. The fits are done using SDSS error bars

(Seljak et al. 2005) reduced by a factor of 10, with the error from simulations added in quadrature.

To obtain an estimate of the minimum reliable scale in simulations, we performed a convergence test with respect to $\Delta\Sigma$, using the low and high resolution (8 times more particles) simulations of cluster CL2 of Tasitsiomi et al. (2004). We found that a reliable minimum scale is $\sim 50 h^{-1} \text{kpc}$ and hence for the fits we only use simulation data on scales larger than that. In fact, resolution can affect both the dark matter density profiles, making them somewhat shallower than they actually are, and the number of subhalos in the innermost host halo regions.

The most striking feature of the figure is how well the halo model reproduces the simulations with 3 free parameters (central halo mass, satellite fraction and satellite radial distribution, assuming that bias is determined by the halo mass, which is confirmed when we compare the fitted values to those predicted). As discussed, the small disagreement on small scales is actually caused by finite resolution in simulations, which leads to an enhancement of $\Delta\Sigma$.

Figure 2 shows the signal from simulations for a combined sample of central and satellite galaxies, such as would be observed in a typical luminosity-selected sample with no additional selections applied. We have also done the fits separately for central and noncentral components. If one takes galaxies in dense regions, then the fraction of satellites is likely to be increased, while if one takes the sample of galaxies in low density regions, the satellite fraction is likely to be decreased. Similar effect can be achieved by color selection; for example, when taking blue galaxies, the satellite fraction is likely to be decreased. These two sub-samples therefore provide the extreme cases of such selection, and are useful as an indication of what additional information one may be able to extract from the g-g lensing data given such selections.

4.1 Central galaxies

There are several aspects of the halo model that we wish to test. We begin with the halo mass distribution for central galaxies. For each of the magnitude bins we have a distribution of central halo masses from the simulations, as shown in figure 3. As is clear from this figure, the halo mass distributions are reasonably narrow in the simulations without scatter, while in the case with scatter they are significantly broader, with the width and asymmetry of the distribution increasing for higher luminosity bins. This effect is also evident from the difference between the mean and the median of the mass distributions given in table 1, which reaches a factor of 5 in the brightest bin with scatter. The width is largest for the brightest bin because the galaxies are on the exponential slope of the luminosity function, while many of the associated halos are on the exponential tail of the halo mass function. In light of the large width, it is difficult to speak of a single mass associated with a given luminosity bin, yet we attempt to determine a single mass using the fitting rather than the full shapes of the curves in Fig. 3, so we must investigate further to understand the consequence of this choice. The relevant questions associated with the halo model fitting are: What is the meaning of the best fit halo mass from the halo model fits? How much of an error is one making by using the best-fit masses if one is interested

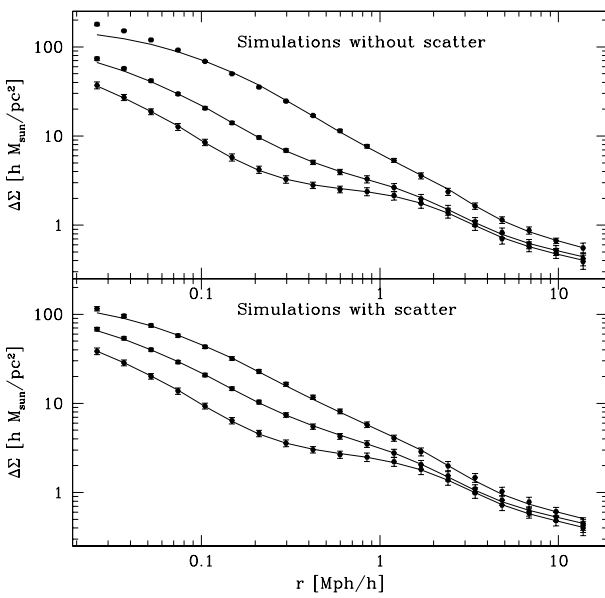


Figure 2. $\Delta\Sigma(r)$ for L3, L4, and L5 luminosity bins, bottom to top. The top panel is for simulations without scatter between V_{\max} and L_r , while the bottom panel is with scatter. Points are the simulation data with errors taken from observations and scaled down by a factor of 10, with simulation errors added in quadrature. The solid line is the halo model fit. Resolution effects become important below $r \approx 50 h^{-1}\text{kpc}$. Thus, for the fits we used simulation data above this scale only; the disagreement for the inner few points is caused by insufficient resolution in simulations.

in the mean (median) halo mass for a given sample? Can one identify from the lensing signal itself the width of the central halo mass distribution?

To address the first two questions, we can compare the mean and median of the distribution to the best-fit masses using a NFW profile. We perform NFW fits in two separate ways. First, we fit the central galaxy component signal only to a NFW profile, using all of the information out to $260 h^{-1}\text{kpc}$. We chose this scale motivated by observational studies where this scale is used to define the aperture mass (e.g., McKay, et al. 2001). We fit simultaneously for concentration and virial mass. In the second case, we use the full combined signal, effectively cutting out the information from the central halos at large transverse separations, since the signal there is dominated by satellites sitting in more massive halos, whose signal dominates at larger radii. In this case we assume concentration c_{dm} based on equation 8, and also fit simultaneously for $b(M_0)$, c_g and α . Both fits give similar results for virial masses (table 1).

If the central galaxy halo mass distribution is narrow, the halo model is able to determine it quite accurately, as shown in table 1. If the halo mass distribution is broad, then there is no typical mass, and in general the g-g lensing mass determination from NFW fits falls between the mean and the median mass of the halo population. If one is interested in the mean halo mass, then the NFW fits underestimate the mass by 10-30% at L3 and 10-55% at L4 and L5, so one must increase the best-fit NFW masses by up to a factor of 2 or even more at the bright end when scatter is significant.

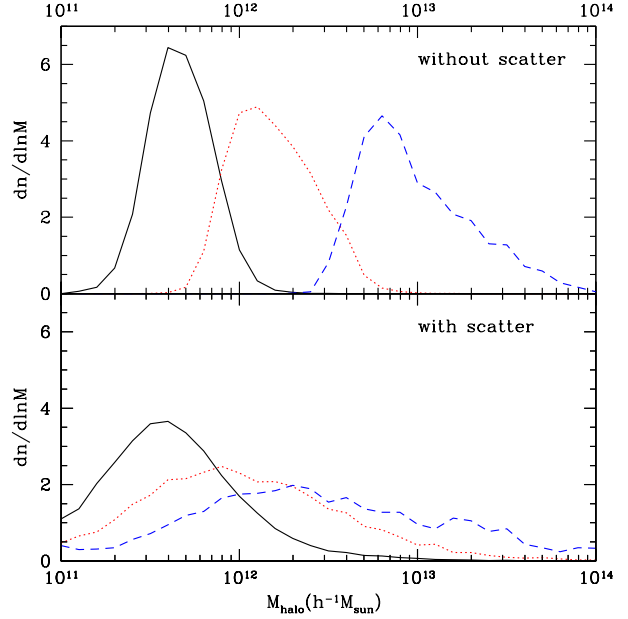


Figure 3. Halo mass distribution for central galaxies for L3 (solid), L4 (dotted), and L5 (dashed) luminosity bins. The top panel is for simulations without scatter, the bottom is with scatter. Median and mean masses are given in table 1.

If the median masses are of more interest, then one must decrease NFW masses by similar amounts. At low luminosities, these corrections are small, but become increasingly important for brighter galaxies because the halo mass distribution is broader. Even more problematic is the fact that it is difficult to assess the corrections from the fits itself, since the fits are good in both cases, but the corrections vary from essentially none in the case without scatter to over a factor of two in the case of scatter. To improve the reliability of the mass determination, one must therefore use samples of galaxies with as little scatter as possible. Below we discuss this point further.

Despite the wide distribution of halo masses, the NFW fitting is able to extract the mean concentration parameters of the dark matter halos correctly. This is particularly true for the lower luminosity cases L3 and L4, where equation 8 with $M_{\text{nl}} = 9 \times 10^{12} h^{-1} M_\odot$ ($\Omega_m = 0.3$, $\sigma_8 = 0.9$) gives $c_{\text{dm}} = 12 - 14$ for the mean virial mass in these bins, in good agreement with the fitted value $c_{\text{dm}} \sim 13$. In L5 without scatter, the fitted value, $c_{\text{dm}} \sim 12$, is somewhat higher than the predicted value $c_{\text{dm}} \sim 10$. It is possible that for this bin, the difference in best-fit masses between the two kinds of fits stems from the assumption of a lower concentration in the fit to the full signal, which would encourage a higher best-fit mass, as is observed. We note here, however, that the NFW dark matter profile is not a perfect fit to the simulations, so there are small differences in the NFW fits to 3-d data versus 2-d $\Delta\Sigma$ data. Hence, these differences may be a reflection of the uncertainties in NFW parameterization rather than a failure of the halo model.

Adding scatter leads to a modest decrease in the fitted concentration parameters. This effect is relatively small in the faintest bin and increases towards the brighter bins, where scatter has more effect. Thus, averaging over 1 mag-

Table 1. Mean and median halo masses for central galaxies in simulations with and without scatter for 3 luminosity bins. Also given are the mass and concentration from NFW profile fits to the g-g lensing signal for the central component only, and using the full (central and satellite) g-g lensing signal. For concentration c_{dm} , we only show the values for the fits to the central component; we assume equation 8 for the fit to the full signal.

Luminosity	$\langle M \rangle_{\text{central}}$	$M_{\text{median,central}}$	$M_{\text{NFWfit,central}}$	$c_{\text{NFWfit,central}}$	$M_{\text{NFWfit,full}}$	Scatter in $V_{\text{max}} - L$
	$10^{12} h^{-1} M_{\odot}$	$10^{12} h^{-1} M_{\odot}$	$10^{12} h^{-1} M_{\odot}$		$10^{12} h^{-1} M_{\odot}$	
L3 [-19,-20]	0.506	0.460	0.476	12.8	0.42 ± 0.03	no
L4 [-20,-21]	1.79	1.47	1.61	12.7	1.52 ± 0.07	no
L5 [-21,-22]	13.2	8.36	9.71	12.2	12.6 ± 0.3	no
L3 [-19,-20]	0.745	0.390	0.579	11.6	0.47 ± 0.04	yes
L4 [-20,-21]	2.91	1.10	1.86	10.9	1.42 ± 0.09	yes
L5 [-21,-22]	11.7	2.34	6.21	10.3	4.8 ± 0.2	yes

Table 2. Fit results from a fit for central halo mass and bias $b(M_0)$ to the signal for central galaxies, using information out to $13h^{-1}\text{Mpc}$. Because neighboring bins are correlated on large scales, the bias errors are likely to be underestimated. The true bias values are from Seljak & Warren (2004).

Luminosity	$M_{\text{NFWfit,central}}$	$b(M_{\text{central}})$	b_{true}	Scatter in $V_{\text{max}} - L$
	$10^{12} h^{-1} M_{\odot}$			
L3 [-19,-20]	0.45 ± 0.02	0.65 ± 0.04	0.68	no
L4 [-20,-21]	1.62 ± 0.03	0.68 ± 0.04	0.72	no
L5 [-21,-22]	11.8 ± 0.2	0.90 ± 0.05	1.00	no
L3 [-19,-20]	0.54 ± 0.02	0.64 ± 0.04	0.68	yes
L4 [-20,-21]	1.82 ± 0.05	0.73 ± 0.04	0.72	yes
L5 [-21,-22]	6.8 ± 0.2	1.00 ± 0.06	0.93	yes

nitude bins in luminosity should allow one to extract the concentration parameter from g-g lensing signal with little or no bias for galaxies below L_* . This is particularly the case if one can identify a galaxy population with a narrow distribution of halo masses. An example of this would be selecting elliptical galaxies that lie in a narrow strip on the fundamental plane which corresponds to the dynamical mass (Padmanabhan et al. 2004). Another example are galaxies selected by stellar mass (Kauffmann, et al. 2003), which is likely to be a more faithful tracer of dynamical mass than the luminosity itself. Careful selection of the lens population in one of these ways, via a reliable tracer of the dynamical mass, should help ensure that the best-fit central halo mass has a simple interpretation.

If one assumes a given cosmological model, then the concentration parameter is fixed, and the difference between the predicted and observed concentration can be used to study the width of the halo mass distribution. We see that even in the cases of a very broad distribution, as in L5, the differences in the average concentration parameter are modest and it will be difficult to observe them directly in observations. Moreover, one can change concentration for a given halo mass by changing the cosmological parameters (primarily nonlinear mass), so the two effects are, to some extent, degenerate.

Table 2 shows results for fits to the central signal using all scales (out to $13h^{-1}\text{Mpc}$) to determine M_0 and bias $b(M_0)$. This determination of b is particularly useful since on large scales the central signal is completely negligible compared to the halo-halo term, so the bias is easily extracted

from the signal amplitude. However, the errorbars are likely underestimated due to the correlations in the correlation function bins. As shown in table 2, the bias values are reasonable for central halos with those masses when compared against the results in Seljak & Warren (2004).

4.2 Satellites

We turn next to the satellite signal. We begin with the distribution of host halo masses for satellites in a given narrow luminosity range. These are very broad, as shown in figure 4. This is expected, since a satellite of a given luminosity can be part of a small group or a large cluster and there is little relation between the halo mass and satellite luminosity. The latter is particularly true for the case with scatter, where the differences between the distributions are very small and only appear at the low mass end of the host halo masses.

Instead of discussing the actual mass distribution we can phrase it in terms of the average halo occupation model, $\langle N(M) \rangle$. To obtain the actual halo mass distribution of satellites, one has to multiply $\langle N(M) \rangle$ with the halo mass function (equation 3). The latter is well determined from simulations for masses in the range $(10^{12} - 10^{14})h^{-1}M_{\odot}$, the range of interest here (Sheth & Tormen 1999; Jenkins et al. 2001). The halo occupation $\langle N(M) \rangle$ as a function of halo mass M is shown in figure 5 for the 3 magnitude bins. We show simulation results without scatter and with scatter. We see that in all cases $\langle N(M) \rangle \propto M$ (i.e., $\epsilon = 1$) is a good fit to the simulations above $3M_0$, while below this mass the number of satellites declines more rapidly. The distributions

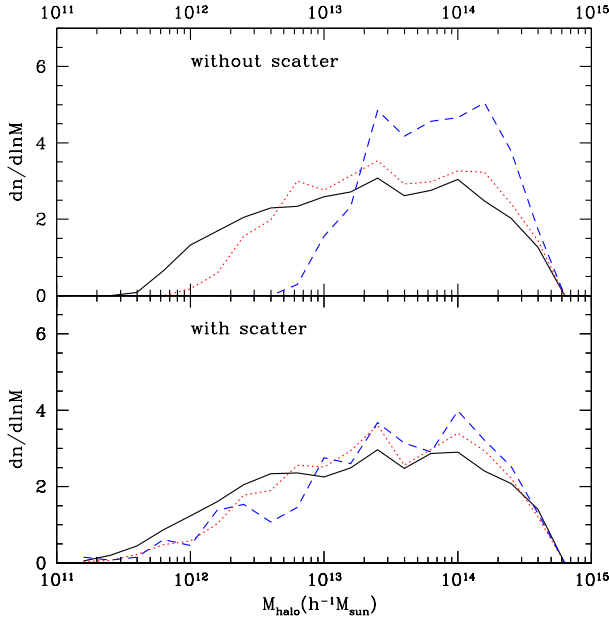


Figure 4. Halo mass distribution for hosts of satellite galaxies for L3 (solid), L4 (dotted), L5 (dashed) luminosity bins. The top panel shows the case where there is no scatter between V_{\max} and L_r , while the bottom panel assumes scatter, as described in § 2. Note that scatter makes the distributions nearly independent of luminosity.

with and without scatter are very similar for L3 and L4, while for L5, the scatter increases the abundance of galaxies at the low mass end. We also show the simple step function model of GS02 and an improved model where the decline below $3M_0$ is more gradual, modeled here as $\langle N(M) \rangle \propto M^2$ below $3M_0$ (the improved model was used for all fits). Note that the overall amplitude is not relevant in these relations, since we normalize it to the overall fraction of the galaxies that are satellites in any given sample.

Examination of figure 2 on ~ 1 Mpc scale shows that scatter has little effect on the noncentral signal in L3 and L4, while for L5 the effect is much more significant: scatter increases the abundance of low mass halos and so reduces the g-g lensing signal. Despite this effect, we are able to reproduce the fraction of satellites in the overall sample rather well: as shown in table 3, the best-fit satellite fractions are in most cases within 10% of the correct value. This quantity therefore appears to be relatively robustly extracted from the data. This works best if we simply ignore the h-h term and only fit out to $2h^{-1}$ Mpc. In a more general fit with the h-h term and out to larger radii, we find there is some degeneracy between the components, and the extracted satellite fraction can be too low in some cases (table 3).

For the halo model, we have to choose the radial distribution of galaxies, which we model as a NFW profile with its own concentration parameter c_g . The concentration of subhalo radial distribution depends sensitively on how the subhalos are selected. Nagai & Kravtsov (2005) show that selection of subhalos by their maximum circular velocity V_{\max} results in concentrations of subhalo number density profiles in clusters in the range $\sim 1.5 - 4$, while selection using luminosity or stellar mass results in considerably larger

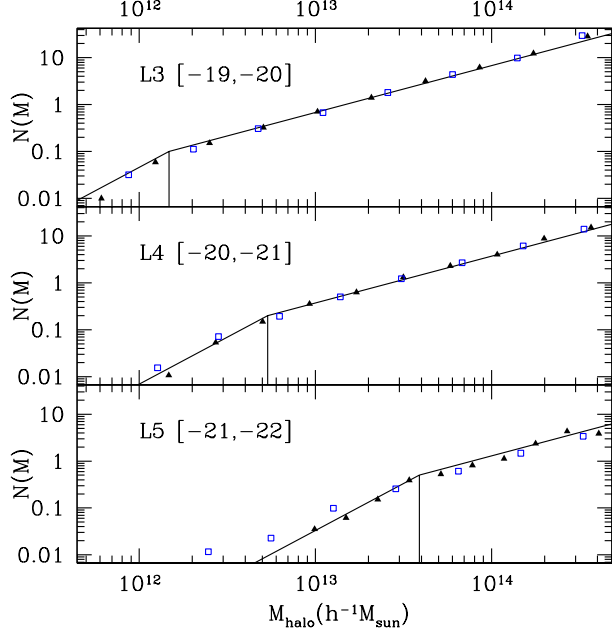


Figure 5. Mean halo occupation number as a function of halo mass for satellite galaxies for the three luminosity bins, as labelled. Solid triangles are without scatter, open squares are with scatter. The solid line is the analytic approximation used here for the halo model, the vertical line delineates the break at $3M_0$ as used in GS02.

concentrations ($c \sim 3 - 10$). Although luminosities have been assigned to the subhalos in our catalogs, the assignment did not take into account the position of the subhalo within its host and depended only on the subhalo's V_{\max} . We can therefore expect that the radial distribution of the cluster subhalos in simulations will be characterized by concentrations similar to those measured for subhalos selected using V_{\max} (i.e., $c_g \sim 1.5 - 4$). Results of our analysis over a broad range of host halo masses, between $10^{12}h^{-1}M_\odot$ to $10^{14}h^{-1}M_\odot$, indeed suggest values of c_g significantly lower than c_{dm} . Table 3 gives the true c_g value from simulations weighted over the halo mass distribution for a given luminosity bin.

It should be noted that shallow profiles for the satellite distribution are not a unique prediction of the simulations. Semi-analytic simulations find $c_g \sim c_{dm}$ by identifying galaxies before merging into larger halos and following their identity even after their surrounding dark matter has been stripped off (Gao et al. 2004). Observations suggest that the galaxy distribution can be well described by the NFW profile in rich clusters (e.g., Carlberg et al. 1997; Lin et al. 2004; Hansen et al. 2004). These works also find that galaxies have concentrations significantly lower than expected for their parent halos. Since the actual value of c_g depends on the physical processes that affect the specific type of galaxy under consideration, we treat c_g as a free parameter to be determined by fitting the simulations (or data).

We find that in order to fit the simulations, we need the satellite distribution to be shallow (table 3), consistent with the value found by directly fitting to the satellite distribution in the same simulations, except for the two high-

Table 3. Satellite fraction and concentration parameter of satellite radial distribution from simulations and from the halo model fits for fits out to $2h^{-1}\text{Mpc}$ without h-h term and out to $13h^{-1}\text{Mpc}$ including the h-h term.

Luminosity	α_{true}	$\alpha_{\text{fit},2h^{-1}\text{Mpc}}$	$\alpha_{\text{fit},13h^{-1}\text{Mpc}}$	c_g,true	$c_g,\text{fit},2h^{-1}\text{Mpc}$	$c_g,\text{fit},13h^{-1}\text{Mpc}$	Scatter in $V_{\text{max}} - L$
L3 [-19,-20]	0.23	0.26 ± 0.03	0.22 ± 0.02	1.5	2.2 ± 1.1	3.2 ± 0.4	no
L4 [-20,-21]	0.20	0.21 ± 0.01	0.18 ± 0.02	3.0	4.7 ± 1.8	5.9 ± 0.7	no
L5 [-21,-22]	0.15	0.15 ± 0.02	0.10 ± 0.02	3.5	1.5 ± 1.3	2.1 ± 0.4	no
L3 [-19,-20]	0.23	0.26 ± 0.03	0.22 ± 0.02	1.5	2.8 ± 1.4	3.9 ± 0.5	yes
L4 [-20,-21]	0.21	0.20 ± 0.02	0.17 ± 0.02	2.5	10 ± 4	12 ± 1	yes
L5 [-21,-22]	0.19	0.16 ± 0.05	0.16 ± 0.03	2.3	20	20	yes

est luminosity bins. As discussed above, the low value of c_g found in simulations does not imply that the same value has to be appropriate to fit the data: the radial distribution of galaxies of a given luminosity inside larger halos is affected by star formation and dynamical processes both before and after falling into the larger halos, which is likely to be quite complicated. What is important for the current discussion is that the halo model should reliably determine the radial distribution of galaxies from the g-g signal, allowing one to determine it from observations.

Table 3 also shows the best-fit value of c_g from the full signal. As shown, even with the ten times reduced SDSS errorbars, we are not highly sensitive to c_g . The result for L5 with scatter is quoted without errorbars because the fit program chose the maximum value allowed in the fits, with very small errorbars. This result (and the high value for L4 with scatter) may be an indication that $\Delta\Sigma$ averaged over such a large range of halo masses does not lend itself well to this type of fitting for a single value of M_0 and c_g . Once again, this result emphasizes that the fitting is most meaningful for groups of lens galaxies chosen to have a narrow distribution in central halo mass, which may not necessarily be the case for *r*-band luminosities even with narrow (1-magnitude wide) bins. The results of the fits suggest that the radial distribution can in principle be extracted from the observations, although we note that when applying this to the actual data, the observational errors were found to be large and unable to provide a strong constraint from the current data samples (Seljak et al. 2005). Note that when the fit was performed to $13h^{-1}\text{Mpc}$ using the combined signal, the bias values $b(M_0)$ were found to be lower than the values in table 2, and an examination of figure 1 suggests that on intermediate scales ($2\text{--}4 h^{-1}\text{Mpc}$), there is some interplay between c_g and $b(M_0)$ that is causing the high best-fit values of c_g and the low values of $b(M_0)$. A better approach may be to determine the bias $b(M_0)$ using the central signal alone as in table 2, then fix it to that value in the fits for the full signal rather than allowing it to vary; this will encourage lower, more reasonable values of c_g .

We note here that the satellite radial distribution is more important for the overall shape of the satellite contribution to g-g lensing signal than the halo occupation number as a function of mass $\langle N(M) \rangle$. Changes in the slope ϵ in $\langle N(M) \rangle \propto M^\epsilon$ mostly change the amplitude of the satellite signal without changing its shape (see figure 7 in GS02). This result is expected, since the satellite signal is dominated by halos with masses in the range $(10^{13} - 10^{14})h^{-1}M_\odot$. Change in the slope changes their relative abundance, but more or less preserves the radial shape of their signal. Consequently,

when we attempted fits for both ϵ and α , the slope ϵ was almost completely degenerate with the fraction of satellites α , but the actual halo mass probability distribution in this mass range was less affected. Hence, as discussed already, we did not fit for ϵ , but instead assumed fixed $\epsilon = 1$ throughout.

Another aspect of the halo model that can be tested with simulations is the amount of dark matter attached to subhalos within the larger halo, though as discussed, we only approach this problem in an average sense. For g-g lensing, the tidal stripping of the outer layers of dark matter attached to the satellite is of little importance, since the lensing signal of that component is swamped by the host halo dark matter signal. In GS02 it was simply assumed that all of the dark matter mass is attached to the subhalo, so that in the inner region, the lensing signal of the satellites is the same as of the central galaxies of the same luminosity. Figure 6, which shows the noncentral signal for one luminosity bin, with the best-fit signal assuming unstripped, moderately stripped, and completely stripped subhalos, shows that this is a good approximation in the inner parts. One should perhaps not be too surprised by this agreement, since by construction in these dissipationless simulations, the galaxies sit on top of subhalos that have survived all the merging and tidal stripping inside the halos. Reality could be more complicated: one could have dark matter in subhalos entirely stripped while the more compact stellar component is preserved.

While the agreement between the simulations and halo model is already good, one can improve the agreement further by modeling the transition between the satellite lensing signal and the host lensing signal, which occurs around $100\text{--}200 h^{-1}\text{kpc}$. We assume that only the dark matter within 0.4 of original virial radius is attached to the satellite (figure 6). This requires that on average 50% of the dark matter is stripped from the satellites. We find the signal to be relatively insensitive to the exact value of truncation radius and consequently g-g lensing cannot be used as a strong probe of tidal stripping process; however, as shown in figure 6, we can exclude the extreme possibility that all halos are fully stripped. To study this issue observationally, it is best to select a galaxy sample with a particularly high satellite fraction α , such as the galaxies in dense environments.

5 CONCLUSIONS

The goal of this paper is to present a detailed comparison of halo model and simulation predictions of galaxy-mass correlations as observed in weak lensing. In its simplest form, and

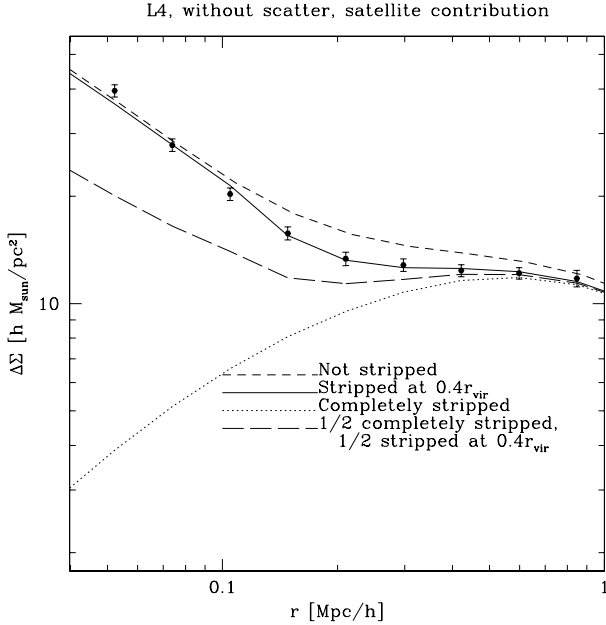


Figure 6. $\Delta\Sigma(r)$ for satellite contribution to $\Delta\Sigma$ from L4 without scatter. The points are from simulations, and the lines are (as labeled) the best-fit signal with no mass stripped, partially stripped (truncation at $0.4r_{vir}$), fully stripped, and a mixture of half partially stripped and half fully stripped.

for a given cosmological model, the halo model has 3 free parameters, which depend on the physics of galaxy formation. These are the typical halo mass of central galaxies (where “typical” is between the median and mean halo mass), the fraction of galaxies that are satellites, and the radial distribution of satellites inside the larger halo.

The halo model provides a fairly accurate description of the g-g lensing signal from simulations, in the sense that it can determine the virial mass distribution of central and non-central galaxies and their relative ratios, as well as the radial distribution of both galaxies and dark matter. One must be careful when interpreting the halo masses from NFW fits if the halo mass distribution is broad as is expected for luminous galaxies ($L > \text{few } L_*$). In this case, g-g lensing is determining something between the mean and the median mass and may not recover the correct radial distribution of the satellite galaxies in their host halos. If one is interested in the mean halo mass, as in the case of application to bias studies (Seljak et al. 2005), then an upward correction needs to be applied; this correction is small at the faint end but can be quite significant at the bright end, especially if there is a significant scatter in the luminosity-halo mass relation.

There are additional parameters that can be added to the description, such as the generalization of the assumed halo mass probability distribution, but they do not improve the fit and are strongly correlated with these 3 parameters. Galaxy-galaxy lensing also allows a determination of the halo mass profile of both central galaxies and satellites. In the latter case, one can constrain the amount of satellite mass stripping inside larger halos, which determined how much dark matter remains attached to the satellites. To investigate the radial profiles of dark matter it is best if one

identifies samples that consist predominantly of central or satellite galaxies, respectively.

Galaxy-galaxy lensing is also quite sensitive to the dark matter concentration parameter c_{dm} , which (in standard cold dark matter models) is not a free parameter but is fixed for any given cosmological model. It varies modestly as a function of cosmology, so in principle one could use this feature to determine the cosmological model. For example, for a typical L_* galaxy with mass around $(1-2) \times 10^{12} h^{-1} M_\odot$, we have $c_{dm} = 12$ in a $\sigma_8 = 0.9$, $\Omega_m = 0.3$ cosmology, which drops to $c_{dm} = 10$ if $\sigma_8 = 0.7$ is used instead. This change is small and we find that it is degenerate with the amount of scatter, which also leads to a lower value of concentration parameter. With current samples, one cannot yet reliably distinguish between these models, but one can test the overall consistency. The accuracy and reliability with which the concentration can be extracted from the data may be improved if galaxies in underdense regions, for which the satellite fraction is lower, are selected. In this case, one can use the signal to a larger distance since it is not swamped by the noncentral component. Concentration can also be determined more accurately with deeper surveys, which can probe dark matter halo at smaller separations (Hoekstra et al. 2004), although modeling angular projection effects in the absence of reliable redshift information for lens galaxies may be difficult.

We find that the data are rather insensitive to the truncation radius of the satellites inside the larger halo as long as it is not very small. We can, however, test the extreme possibility that satellites have no dark matter attached to them. This is unlikely to be the case for all satellites even though it may be valid for some fraction of those near the center. For example, Gao et al. (2004) argue that up to 40% of galaxies in clusters may not have associated DM halos, a conjecture which may be testable with the future weak lensing measurements (see Fig. 6).

Additional information about the galaxy-dark matter halo connection may be more challenging to extract from the data. For example, we have assumed that the number of satellites inside the halo scales linearly with halo mass. If this assumption is dropped and a more general power law relation is allowed, a degeneracy is developed between the satellite fraction and the power law slope, but the overall fraction of galaxies in $(10^{13} - 10^{14}) h^{-1} M_\odot$ halos is preserved.

We note here that the power law slope and other parameters may be constrained by other observations such as the galaxy auto-correlation function analysis, velocity information in redshift surveys and direct counting of galaxies in groups and clusters. In fact, a halo model similar to the one used here was applied to the galaxy auto-correlation analysis (Zehavi, et al. 2004). Combining and comparing the two data sets should provide important consistency checks and will further constrain the galaxy-dark matter connection.

ACKNOWLEDGEMENTS

RM is supported by the NSF Graduate Research Fellowship Program (NSF GRFP). US is supported by a fellowship from the David and Lucile Packard Foundation, NASA grants NAG5-1993, NASA NAG5-11489 and NSF grant CAREER-0132953. AVK and AT are supported by the National Science Foundation (NSF) under grants No. AST-0206216 and

AST-0239759, by NASA through grants NAG5-13274 and NAG5-12326, and by the Kavli Institute for Cosmological Physics at the University of Chicago. RHW is supported by NASA through a Hubble Fellowship awarded by the Space Telescope Science Institute, which is operated by the Association of Universities for Research in Astronomy, Inc., for NASA, under contract NAS 5-26555. The simulations used in this study were performed on the IBM RS/6000 SP3 system at the National Energy Research Scientific Computing Center (NERSC).

REFERENCES

Blanton M. R., et al., 2003, *ApJ*, 592, 819
 Brainerd T. G., Blandford R. D., Smail I., 1996, *ApJ*, 466, 623
 Bullock J. S., Kolatt T. S., Sigad Y., Somerville R. S., Kravtsov A. V., Klypin A. A., Primack J. R., Dekel A., 2001, *MNRAS*, 321, 559
 Carlberg R. G., Yee H. K. C., Ellingson E., 1997, *ApJ*, 478, 462+
 Cooray A., Sheth R., 2002, *Phys.Rep.*, 372, 1
 Eke V. R., Navarro J. F., Steinmetz M., 2001, *ApJ*, 554, 114
 Fischer P., et al., 2000, *AJ*, 120, 1198
 Gao L., De Lucia G., White S. D. M., Jenkins A., 2004, *MNRAS*, 352, L1
 Gao L., White S. D. M., Jenkins A., Stoehr F., Springel V., 2004, *MNRAS*, pp 484–+
 Ghigna S., Moore B., Governato F., Lake G., Quinn T., Stadel J., 1998, *MNRAS*, 300, 146
 Ghigna S., Moore B., Governato F., Lake G., Quinn T., Stadel J., 2000, *ApJ*, 544, 616
 Gnedin O. Y., Kravtsov A. V., Klypin A. A., Nagai D., 2004, *ApJ*, 616, 16
 Guzik J., Seljak U., 2001, *MNRAS*, 321, 439
 Guzik J., Seljak U., 2002, *MNRAS*, 335, 311
 Hansen S. M., McKay T. A., Wechsler R. H., Annis J., Sheldon E. S., Kimball A., 2004, *ApJ* submitted (astro-ph/0410467)
 Hirata C. M., et al., 2004, *MNRAS*, 353, 529
 Hoekstra H., Franx M., Kuijken K., Carlberg R. G., Yee H. K. C., 2003, *MNRAS*, 340, 609
 Hoekstra H., Yee H. K. C., Gladders M. D., 2004, *ApJ*, 606, 67
 Hudson M. J., Gwyn S. D. J., Dahle H., Kaiser N., 1998, *ApJ*, 503, 531+
 Jenkins A., Frenk C. S., White S. D. M., Colberg J. M., Cole S., Evrard A. E., Couchman H. M. P., Yoshida N., 2001, *MNRAS*, 321, 372
 Kauffmann G., Colberg J. M., Diaferio A., White S. D. M., 1999, *MNRAS*, 303, 188
 Kauffmann G., et al., 2003, *MNRAS*, 341, 33
 Klypin A., Gottlöber S., Kravtsov A. V., Khokhlov A. M., 1999, *ApJ*, 516, 530
 Kravtsov A. V., Berlind A. A., Wechsler R. H., Klypin A. A., Gottlöber S., Allgood B., Primack J. R., 2004, *ApJ*, 609, 35
 Kravtsov A. V., Gnedin O. Y., Klypin A. A., 2004, *ApJ*, 609, 482
 Kravtsov A. V., Klypin A. A., 1999, *ApJ*, 520, 437
 Kravtsov A. V., Klypin A. A., Khokhlov A. M., 1997, *ApJS*, 111
 Lin Y., Mohr J. J., Stanford S. A., 2004, *ApJ*, 610, 745
 McKay T. A., et al., 2001, *astro-ph/0108013*
 Nagai D., Kravtsov A. V., 2005, *ApJ*, 618, 557
 Navarro J. F., Frenk C. S., White S. D. M., 1996, *ApJ*, 462, 563+
 Padmanabhan N., et al., 2004, *New Astronomy*, 9, 329
 Press W. H., Schechter P., 1974, *ApJ*, 187, 425
 Seljak U., 2000, *MNRAS*, 318, 203
 Seljak U., Makarov A., Mandelbaum R., Hirata C. M., Padmanabhan N., McDonald P., Blanton M. R., Tegmark M., Bahcall N. A., Brinkmann J., 2005, *Phys.Rev.D*, 71, 043511
 Seljak U., Warren M. S., 2004, *MNRAS*, 355, 129
 Sheldon E. S., Johnston D. E., Frieman J. A., Scranton R., McKay T. A., Connolly A. J., Budavári T., Zehavi I., Bahcall N. A., Brinkmann J., Fukugita M., 2004, *AJ*, 127, 2544
 Sheth R. K., Mo H. J., Tormen G., 2001, *MNRAS*, 323, 1
 Sheth R. K., Tormen G., 1999, *MNRAS*, 308, 119
 Smith D. R., Bernstein G. M., Fischer P., Jarvis M., 2001, *ApJ*, 551, 643
 Spergel D. N., et al., 2003, *ApJS*, 148, 175
 Tasitsiomi A., Kravtsov A. V., Gottlöber S., Klypin A. A., 2004, *ApJ*, 607, 125
 Tasitsiomi A., Kravtsov A. V., Wechsler R. H., Primack J. R., 2004, *ApJ*, 614, 533
 Tegmark M., et al., 2004, *Phys.Rev.D*, 69, 103501
 Tyson J. A., Valdes F., Jarvis J. F., Mills A. P., 1984, *ApJ*, 281, L59
 Warren M. S., Abazajian, K., Holz, D. E., Teodoro, L., 2005, *astro-ph/0506395*
 Weinberg D. H., Davé R., Katz N., Hernquist L., 2004, *ApJ*, 601, 1
 Weller J., Ostriker J. P., Bode P., 2004, *ApJ* submitted (astro-ph/0405445)
 White M., 2001, *A&A*, 367, 27
 Yahagi H., Nagashima M., Yoshii Y., 2004, *ApJ*, 605, 709
 Yang X. H., Mo H. J., Kauffmann G., Chu Y. Q., 2003, *MNRAS*, 339, 387
 Zehavi I., et al., 2004, *astro-ph/0408569*